Single Electron on a Nanodot in a Double-Barrier Tunneling Structure Observed by Noncontact Atomic-Force Spectroscopy

Yasuo Azuma
Department of Physical Electronics, Tokyo Institute of Technology, Tokyo 152-8552, Japan

Masayuki Kanehara and Toshiharu Teranishi
Graduate School of Pure and Applied Sciences, University of Tsukuba, 1-1-1 Tennodai, Tsukuba, Ibaraki 305-8571, Japan

Yutaka Majima*
Department of Physical Electronics, Tokyo Institute of Technology and SORST, Japan Science and Technology Agency, Tokyo 152-8552, Japan

(Received 28 October 2005; published 12 January 2006)

A single electron has been observed on a nanodot in a double-barrier tunneling structure by noncontact atomic-force microscopy at fixed separation. Frequency shift-voltage dependence of an Au-coated cantilever/vacuum/1-decanethiol protected Au nanodot/1-octanethiol self-assembled monolayer/Au substrate structure deviates from the theoretical parabolic curve, which is attributed to the change in the number of quantized electrons on the Au nanodot caused by the Coulomb blockade phenomena.

DOI: 10.1103/PhysRevLett.96.016108 PACS numbers: 81.07.−b, 07.79.Lh, 73.23.Hk

Nanomechanical single-electron devices have attracted considerable attention due to their interesting phenomena and are expected to function as novel devices in the field of nanoelectronics [1–8]. In nanometer-sized double-barrier tunneling structures, electron tunneling is restrained and a number of electrons on Coulomb islands are quantized due to Coulomb blockade (CB) phenomena. It should be noted that the polarity of the number of electrons on a Coulomb island strongly depends on the ratio of the tunneling resistance between the Coulomb island and two reservoirs [9,10]. In these double-barrier tunneling structures, electron transport can be modulated when soft organic links that enable Coulomb islands to vibrate are introduced as tunneling barriers [1].

For better understanding the operation of nanomechanical single-electron devices, the observation of a single electron on a nanodot in a double-barrier tunneling structure is important. We have developed a simultaneous measurement system based on scanning tunneling microscopy to measure the displacement current and tunneling current; a scanning vibrating probe is used in this system [11–14]. By using this system, we have observed the motion of electrons on Coulomb islands by measuring the displacement current staircase using an electrical method [9,10,15]. Further, several methods for measuring the electrostatic force by atomic-force microscopy (AFM) have been proposed in order to study charges on a sample surface [16–18]. Atomic-force spectroscopy (AFS) is a highly sensitive technique for detecting the electrostatic force; this technique employs the frequency modulation (FM) detection method of noncontact AFM (nc-AFM) in ultrahigh vacuum (UHV) [19,20].

In this Letter, we measure the cantilever frequency shift (Δf)-sample voltage (V_S) characteristic in a double-barrier tunneling structure that consists of an Au-coated cantilever/vacuum/1-decanethiol [$CH_3(CH_2)_9SH$, C10S] protected Au nanodot (C10S-Au nanodot)/1-octanethiol [$CH_3(CH_2)_7SH$, C8S] self-assembled monolayer (SAM)/Au substrate. We demonstrate and discuss single-electron counting on a C10S-Au nanodot caused by the CB phenomena.

The sample that comprises C10S-Au nanodots on an Au substrate is fabricated as follows. The Au substrate is prepared by a vacuum evaporation method onto cleaved mica. Before the evaporation, mica is heated at 673 K for 1 h. The postanneal is fabricated at 623 K for 8 h to form an atomically flat Au(111) surface. The Au substrate is then immersed in a solution of C8S in ethanol for 48 h to form a SAM. C10S-Au nanodots are spread on C8S SAM by adding a solution of C10S-Au nanodots to toluene. The diameter of the Au core is estimated to be 3.3 ± 0.6 nm from the transmission electron microscope image [21]. The typical cantilever resonant frequency and tip radius are 315 kHz and 50 nm, respectively.

Figure 1 shows the experimental setup based on UHV nc-AFM for measuring the frequency shift Δf-sample voltage V_S characteristic. When an electron tunnels on the Au core of a nanodot, the number of electrons on the nanodot varies; this results in the addition of an electrostatic force on the cantilever. The electrostatic force thus applied V_S is measured from the Δf-V_S characteristic. Throughout the experiment, the vacuum pressure is maintained below 3×10^{-8} Pa and the measurements are carried out at 100 K.

Figure 2 shows the typical series of Δf-V_S measurements of the C8S SAM/Au (111) sample without C10S-Au nanodots; these measurements were carried out in the voltage range of -1 to 1 V by changing the z-axis position

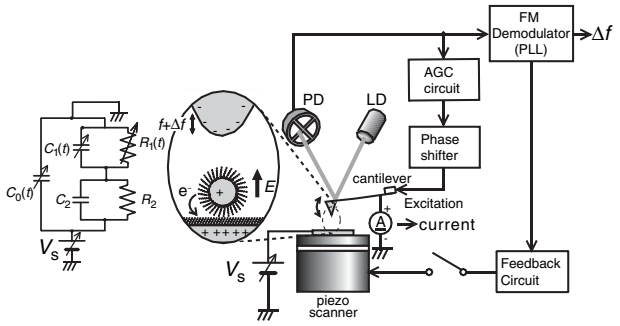

FIG. 1. Experimental setup of atomic-force spectroscopy. Equivalent circuit is also shown. C_1 and R_1 denote the capacitance and tunneling resistance between the Au cantilever and Au core, respectively, and C_2 and R_2 denote the capacitance and tunneling resistance between the Au core and Au substrate, respectively. C_0 is the capacitance between the Au cantilever and Au substrate. Laser diode, photodiodes, autogain controller, and phase lock loop are denoted as LD, PD, AGC, and PLL, respectively.

of the cantilever in steps of 1 nm successively. As shown in Fig. 2, the Δf-V_S characteristics become parabolic curves and have a peak at a voltage of 0.50 V, which corresponds to the contact potential difference V_d. During the measurement, the separation and the amplitude are maintained within ± 0.05 nm and at 5.00 ± 0.01 $\mathrm{nm_{p\text{-}p}}$, respectively.

An nc-AFM image of C10S-Au nanodots on the sample is shown in the inset of Fig. 3. From this image, their diameter is estimated to be 7 nm. Since the length of C10S and the diameter of the core are 1.7 nm and 3.3 ± 0.6 nm [21,22], respectively, the typical diameter of the C10S-Au nanodot should be approximately 6.5 nm. This diameter of 6.5 nm agrees with the diameter of the observed C10S-Au nanodots in the nc-AFM image. The

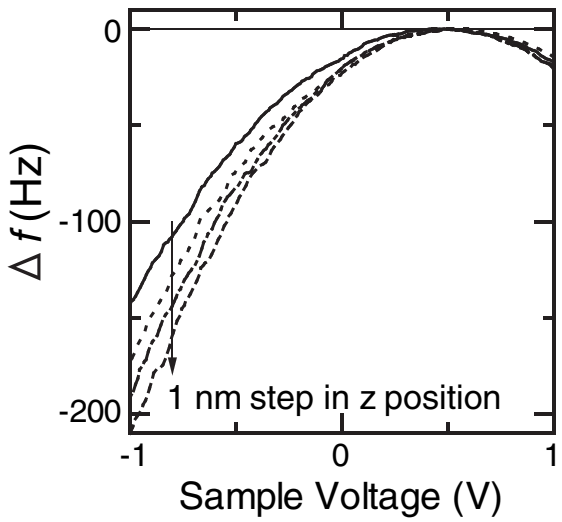

FIG. 2. Δf-V_S dependence on C8S SAM without C10-Au nanodot, obtained by changing the z-axis position of the cantilever.

density of C10S-Au nanodots was approximately 560 $\mu\mathrm{m}^{-2}$.

Figure 3(a) shows the Δf-V_S characteristic of the C10S-Au nanodot at the crossing point in the AFM image in the voltage range of -1 to 1 V. In Fig. 3(a), the Δf-V_S dependence resembles a parabolic curve. V_d is evaluated as 0.17 V from the peak voltage in the Δf-V_S characteristic. Because of the electrostatic force of attraction between the Au cantilever and Au substrate, Δf decreases as V_S becomes different from V_d. During the measurement, the average cantilever position and the cantilever oscillation amplitude are maintained at less than 0.04 nm and 3.62 ± 0.01 $\mathrm{nm_{p\text{-}p}}$, respectively. It is noteworthy that two kinks are clearly observed at V_S of -0.62 and 0.70 V. The tunneling current is not observed within the current level of ± 200 fA, as shown in Fig. 3(b).

The free energy consists of the electrostatic charging energy, and the work done by the voltage source, U, can be expressed as [20]

$$U = \frac{q^2}{2C_\Sigma} - \frac{C_1}{2C_\Sigma} Vq - \frac{C_1 C_2}{2C_\Sigma} V^2 - \frac{C_0}{2} V^2, \qquad (1)$$

where V is the voltage of $(V_S - V_d)$, q is the charge residing in the Au core, C_Σ is the sum of the tip-Au core C_1 and the Au core-substrate C_2 capacitances, and C_0 is the

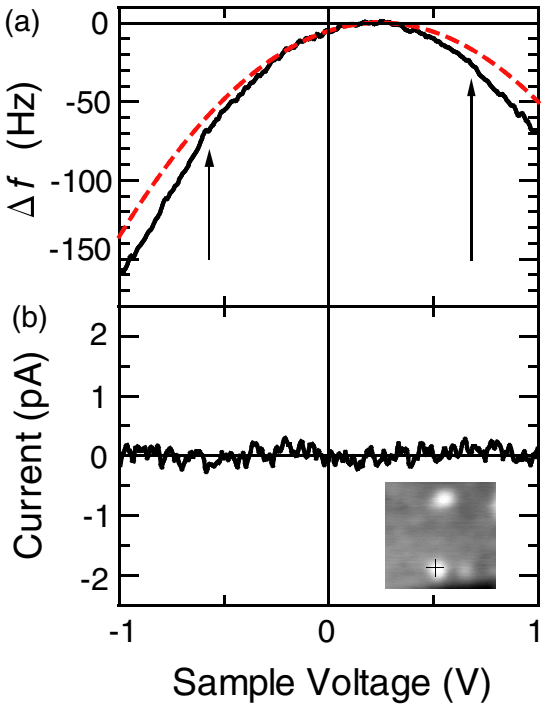

FIG. 3 (color online). (a) Experimental Δf-V_S characteristic of a double-barrier tunneling structure (solid line). The dashed line shows the theoretical parabolic curve calculated by using the least-square method in the voltage range of $-0.15 < V_S < 0.15$ V. (b) Tunneling current-sample voltage characteristic. Inset: nc-AFM image of the sample (60×60 $\mathrm{nm^2}$). Δf-V measurement is performed on top of the single C10S-Au dot indicated in this image.

cantilever-substrate capacitance. The electrostatic force acting on the tip, F, is given by differentiating U with respect to the vertical position z ($F = -\partial U/\partial z$), as follows:

$$F = \frac{1}{C_\Sigma^2}\frac{\partial C_1}{\partial z}\left[\frac{q^2}{2} - C_2 V q + \frac{C_2^2 V^2}{2}\right] + \frac{1}{2}\frac{\partial C_0}{\partial z}V^2. \quad (2)$$

The first term is derived from the charge in the Au core and its image charge on the tip; however, it is negligibly small under the experimental conditions [20]. The second term is derived from the charge in the Au core and the polarized charge on the tip. The third and fourth terms are derived from the polarized charges of the tip substrate and cantilever substrate, respectively; these terms have parabolic characteristics.

Since the cantilever oscillates at the resonant frequency f_0, the position z can be expressed as $z = d_0 + A_0[1 + \cos(2\pi f t)]$, where d_0 is the least distance between the Au cantilever and Au substrate, A_0 is the cantilever oscillation amplitude, and f is cantilever vibrating frequency. The frequency shift Δf ($= f_0 - f$) is given by the following equation according to the first-order perturbation theory [23]:

$$\Delta f = -\frac{f_0^2}{kA_0}\int_0^{1/f_0} Fz\cos(2\pi f_0 t)dt, \quad (3)$$

where k is the Au cantilever spring constant. Δf is expressed as

$$\Delta f = \Delta f_1 + \Delta f_{\mathrm{CB}}, \quad (4)$$

where Δf_1 is the frequency shift caused by the sum of the third and fourth terms and Δf_{CB} is the frequency shift caused by the second term in Eq. (2). Since the third and fourth terms are proportional to $(V_S - V_d)^2$ in Eq. (2), Δf_1 tends to be proportional to $(V_S - V_d)^2$. Therefore, Δf_{CB} is calculated by subtracting Δf_1 from Δf and is expressed as $\Delta f_{\mathrm{CB}} = \Delta f - \alpha(V_S - V_d)^2$. In the Coulomb gap, it is noted that Δf_{CB} becomes zero because $q = 0$. Therefore, the parameter α can be evaluated by fitting the theoretical term of $\alpha(V_S - V_d)^2$ into the measurement curve of Δf-V_S characteristic within the Coulomb gap.

Figures 4(a) and 4(b) show the normalized capacitance $C/4\pi\varepsilon r$ and differentiation of $C/4\pi\varepsilon r$ with respect to the dependence of the normalized position (z/r) observed in the mirror image of a point-charge model of a charged sphere (radius r) at the distance x below the conducting plate [24]. It should be noted that the capacitance C is proportional to $4\pi\varepsilon r$, which is equal to the capacitance of the sphere with radius r in free space. By assuming a radius of 1.7 nm, a separation of 1.7 nm, and the relative permittivity of C10S as 2.6 [25,26], the minimum Coulomb step width $\Delta = e/C_1$ becomes 0.25 V.

Single-electron charging in an individual InAs quantum dot has been demonstrated by Stomp *et al.* [20]. Based on experimental Δf-V_S characteristics, they evaluated the voltage width between two kinks as 3Δ. In Fig. 3(a), the

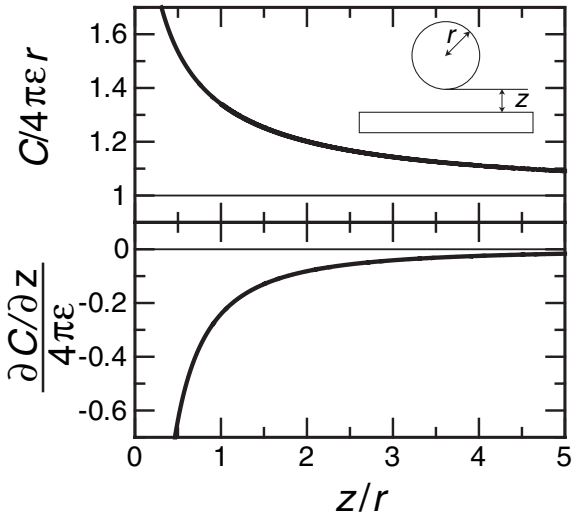

FIG. 4. (a) Normalized capacitance $C/4\pi\varepsilon r$ and (b) differentiation of $C/4\pi\varepsilon r$ with respect to the dependence of the normalized position (z/r) in the mirror image point-charge model of a charged sphere (radius r) at distance x below the conducting plate.

voltage width between the two kinks is 1.32 V. By considering the theoretical minimum Coulomb step width of 0.25 V, a voltage step width of 1.32 V should be attributed to 3Δ. The theoretical parabolic curve is calculated by using the least-square method in the voltage range of $-0.15 < V_S < 0.15$ V, which is almost equal to the theoretical minimum Coulomb step width (broken line in Fig. 3(a)]. Further, α and V_d are obtained as -88 Hz/V^2 and 0.24 V, respectively.

Figure 5(a) shows the experimental Δf_{CB}-V_S curve. Since an attractive force is applied on the Au cantilever in the voltage ranges of approximately $V_S < -0.2$ V and $V_S > 0.3$ V, the polarity of the number of electrons on the Au core is opposite to that of the charge on the Au cantilever. This indicates that the tunneling resistance between the Au cantilever and Au core (R_1) is greater than that between the latter and the Au substrate (R_2) [9,10]. According to the full orthodox theory for a two-junction system, the tunneling processes across the junctions can be derived from a basic golden rule calculation. Hence, the average number of electrons on the Au core, $n(V_S)$ [$= q/e$, where e is the unit charge ($e > 0$)], can be calculated by assuming the following parameters: R_1, C_1, R_2, C_2, and the fractional residual charge Q_0 [24,27,28]. Assuming that $3\Delta = 1.32$ V, C_1 becomes 0.36 aF. The theoretical $n(V_S)$ curve as shown in Fig. 5(b) is obtained using the following parameter values: $R_1/R_2 = 50$, $C_1 = 0.36$ aF, $C_2 = 0.34$ aF, and $Q_0 = -0.092e$. In Fig. 5(a), the theoretical electrostatic force F_{CB} due to the charge in the Au core and the polarized charge on the tip is also shown; here it is assumed that $(\partial C/\partial z)/(4\pi\varepsilon) = 0.12$ ($z/r = 1.5$). It is evident that the theoretical F_{CB} agrees well with the experimental Δf_{CB}-V_S curve. Consequently, the Δf_{CB}-V_S dependence can be attributed to CB phenomena. The frac-

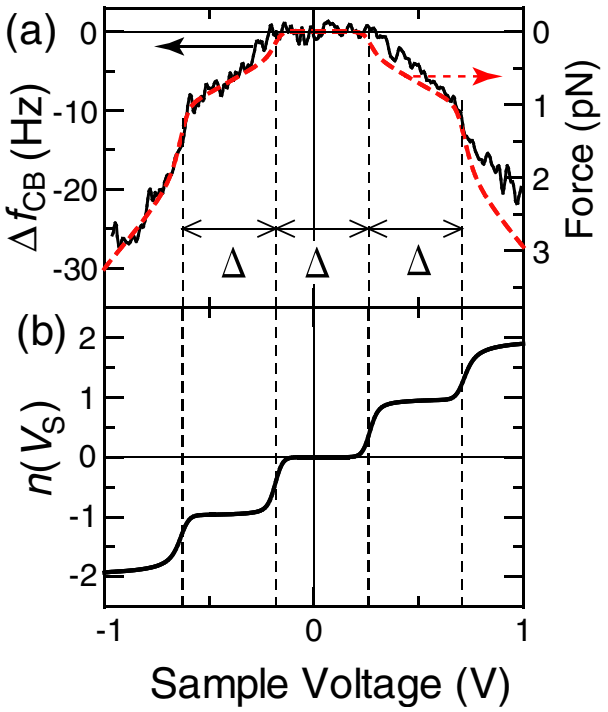

FIG. 5 (color online). (a) Frequency shift caused by the CB (Δf_{CB})-V_S curve (solid line). Theoretical electrostatic force F_{CB} from the charge in the Au core and the polarized charge on the tip by assuming $(\partial C/\partial z)/(4\pi\varepsilon) = 0.12$ $(z/r = 1.5)$ (dashed line). (b) Theoretical $n(V_S)$ curve obtained for parameter values of $R_1/R_2 = 50$, $C_1 = 0.36$ aF, $C_2 = 0.34$ aF, and $Q_0 = -0.092e$.

tional charge Q_0 of $-0.092e$ is attributed to the 40 mV shift of the Coulomb staircase. It is noted that the voltage shift of the Coulomb staircase is independent of V_d; this is because V_d is estimated as 0.24 V.

In conclusion, Δf-V_S characteristics have been measured in a double-barrier tunneling structure that consists of an Au-coated cantilever/vacuum/1-decanethiol protected Au nanodot (C10S-Au nanodot)/1-octanethiol self-assembled monolayer (SAM)/Au substrate. Further, the charging of a single electron on a colloidal Au nanodot due to Coulomb blockade phenomena has been observed by the AFS technique. This study is significant for the development of nanomechanical single-electron devices such as electron shuttle devices with self-excitation by using a colloidal nanodot.

This work is partially supported by the 21st Century COE Program, Photonics Nanodevice Integration Engineering by the Ministry of Education, Culture, Sports, Science and Technology (MEXT), Industry Technology Research Grant Program in 2004 by NEDO, and Grant-in-Aid for Young Scientists (A) (No. 15681009) by MEXT, Japan.

*Corresponding author.
Electronic address: majima@pe.titech.ac.jp

[1] L. Y. Gorelik, A. Isacsson, M. V. Voinova, B. Kasomo, R. I. Shekhter, and M. Jonson, Phys. Rev. Lett. **80**, 4526 (1998).
[2] H. Park, J. Park, A. K. L. Lim, E. H. Anderson, A. P. Alivisatos, and P. L. McEuen, Nature (London) **407**, 57 (2000).
[3] A. Erbe, C. Weiss, W. Zwerger, and R. H. Blick, Phys. Rev. Lett. **87**, 096106 (2001).
[4] Y. Xue and M. A. Ratner, Phys. Rev. B **68**, 235410 (2003).
[5] R. G. Knobel and A. N. Cleland, Nature (London) **424**, 291 (2003).
[6] M. D. Lahaye, O. Buu, B. Camarota, and K. C. Shwab, Science **304**, 74 (2004).
[7] A. D. Armour, M. P. Blencowe, and Y. Zhang, Phys. Rev. B **69**, 125313 (2004).
[8] Y. Majima, Y. Azuma, and K. Nagano, Appl. Phys. Lett. **87**, 163110 (2005).
[9] Y. Majima, K. Nagano, and A. Okuda, Jpn. J. Appl. Phys. **41**, 5381 (2002).
[10] K. Nagano, A. Okuda, and Y. Majima, Appl. Phys. Lett. **81**, 544 (2002).
[11] Y. Majima, Y. Oyama, and M. Iwamoto, Phys. Rev. B **62**, 1971 (2000).
[12] Y. Majima, S. Miyamoto, Y. Oyama, and M. Iwamoto, Jpn. J. Appl. Phys. **37**, 4557 (1998).
[13] Y. Oyama, Y. Majima, and M. Iwamoto, J. Appl. Phys. **86**, 7087 (1999).
[14] Y. Majima, S. Uehara, T. Masuda, A. Okuda, and M. Iwamoto, Thin Solid Films **393**, 204 (2001).
[15] Y. Azuma, K. Nagano, and Y. Majima, Jpn. J. Appl. Phys. **42**, 2458 (2003).
[16] Y. Sugawara, T. Uchihashi, M. Abe, and S. Morita, Appl. Surf. Sci. **140**, 371 (1999).
[17] Y. Suganuma, P.-E. Trudeau, and A.-A. Dhirani, Phys. Rev. B **66**, 241405 (2002).
[18] L. J. Klein and C. C. Williams, Appl. Phys. Lett. **81**, 4589 (2002).
[19] T. Arai and M. Tomitori, Phys. Rev. Lett. **93**, 256101 (2004).
[20] R. Stomp, Y. Miyahara, S. Schaer, Q. Sun, H. Guo, P. Grutter, S. Studenikin, P. Poole, and A. Sachrajda, Phys. Rev. Lett. **94**, 056802 (2005).
[21] T. Teranishi, S. Hasegawa, T. Shimizu, and M. Miyake, Adv. Mater. **13**, 1699 (2001).
[22] N. Gamillone III, T. Y. B. Leung, P. Schwartz, P. Eisenberger, and G. Scoles, Langmuir **12**, 2737 (1996).
[23] F. J. Giessibl, Phys. Rev. B **56**, 16 010 (1997).
[24] H. Zhang, Y. Yasutake, Y. Shichibu, T. Teranishi, and Y. Majima, Phys. Rev. B **72**, 205441 (2005).
[25] M. D. Porter, T. B. Bright, D. L. Allara, and C. E. D. Chidsey, J. Am. Chem. Soc. **109**, 3559 (1987).
[26] M. A. Rampi, O. J. A. Schueller, and G. M. Whitesides, Appl. Phys. Lett. **72**, 1781 (1998).
[27] A. E. Hanna and M. Tinkham, Phys. Rev. B **44**, 5919 (1991).
[28] D. V. Averin and K. K. Likharev, *Mesoscopic Phenomena in Solids*, edited by B. L. Altshuler, P. A. Lee, and R. A. Webb (Elsevier, Amsterdam, 1991), p. 169.